Compensation of Gravity-induced Errors on Hexapod-type Parallel Mechanism Machine Tools

Masao Nakagawa, Tetsuya Matsushita and Tomoharu Ando
Department of Research and Development, Okuma Corporation
Oguchi-cho, Aichi 480-0193, Japan
E-mail: m-nakagawa@gmx.okuma.co.jp
Yoshiaki Kakino, Soichi Ibaraki and Hiroya Takaoka
Department of Precision Engineering, Kyoto University
Sakyo-ku, Kyoto 606-8501, Japan
E-mail: kakino@prec.kyoto-u.ac.jp

Summary

This paper proposes a motion error compensation methodology for a Hexapod-type parallel mechanism machine tool. First, the contouring error attributable to the elastic deformation of struts caused by the gravity is predicted for an arbitrary position and orientation of spindle head. By compensating the predicted error on a reference trajectory, the machine's motion accuracy can be improved. It is experimentally verified that predicted and measured motion trajectories coincide well, even when the spindle is tilted by more than 23 degrees, where the gravity significantly deteriorates the machine's motion accuracy. By applying the proposed compensation method, the motion accuracy is significantly improved particularly near an edge of the machine's workspace.
Keywords: Hexapod machine tool, Accuracy calibration, Motion accuracy, Double Ball Bar, Gravity error

1. Introduction

Although six-axis machine tools of the "Hexapod" type mechanism are now commercially available, they are not widely accepted in today's industry. A critical, and inherent problem of a Hexapod-type machine tool is its low stiffness. Another issue is on their motion accuracies, particularly on the calibration of kinematic parameters and the compensation of motion errors.

In our previous work[(1)], we presented a calibration methodology that performs DBB[(2)] measurements under the condition where a tilting angle of the spindle is small, and thus the elastic deformation of struts due to the platform weight is minimized. By applying the proposed method, the circularity error was reduced to as small as 8 μm, when the spindle is near the center of the workspace. However, when the spindle is near an edge of the workspace and is tilted, or its tilting angle is very large even though the spindle is near the center of the workspace, the elastic deformation of struts caused by the gravity imposes a significant effect on the machine's contouring performance. As a result, the circularity error becomes as much as 40~140 μm in such a case.

Conventional serial mechanism machine tools also worsen their motion accuracy near an edge of the workspace or when the tilting angle is larger. In the case of a parallel mechanism machine, it is mainly due to the elastic deformation of mechanical parts. If the effect of the gravity can be predicted and compensated, the motion accuracy can be significantly improved all over the workspace. Weck et al.[(3)] presented a compensation method for the axial deformation of struts on the Stewart platform. Soons et al. [(4)] discussed the positioning error at the tool tip due to the elastic deformation on a parallel mechanism machine.

It should be emphasized that the motion error due to the miscalibration of kinematic parameters must be minimized in order for an effective gravity compensation. When the kinematic parameters are calibrated in a sufficient accuracy, the motion error due to the gravity can be predicted by using a simulation model of the elastic deformation of the parallel mechanism. By using this simulation result, the reference trajectory is compensated to improve the machine's overall motion accuracy.

2. Configuration of a Hexapod-type Machine Tool

This paper considers a Hexapod-type parallel mechanism machine tool of the Stewart platform[(5)] depicted in Figure 1. It has six telescoping struts, each of which is connected to the base by a 2-DOF (degrees of freedom) joint. The other end of each strut is connected by a 3-DOF joint to the platform, where a machine spindle is installed.

Figure 1 shows a schematic view of COSMO CENTER PM-600, a Hexapod-type machine tool[(6)] used in our study. Table 1 shows its major specifications

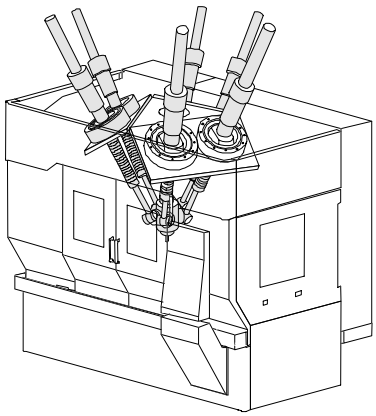

Fig. 1 COSMO CENTER PM-600

Table 1 Specifications of PM-600

Travels(X,Y,Z) [mm]	φ600(XY) × 400(Z) 420 × 420 × 400
Tilting angle [°]	± 25
Rapid traverse [m/min]	100
Max. acceleration [m/s^2]	14.7
Spindle speed [min^{-1}]	12,000 / 30,000
Spindle motor [kW]	6

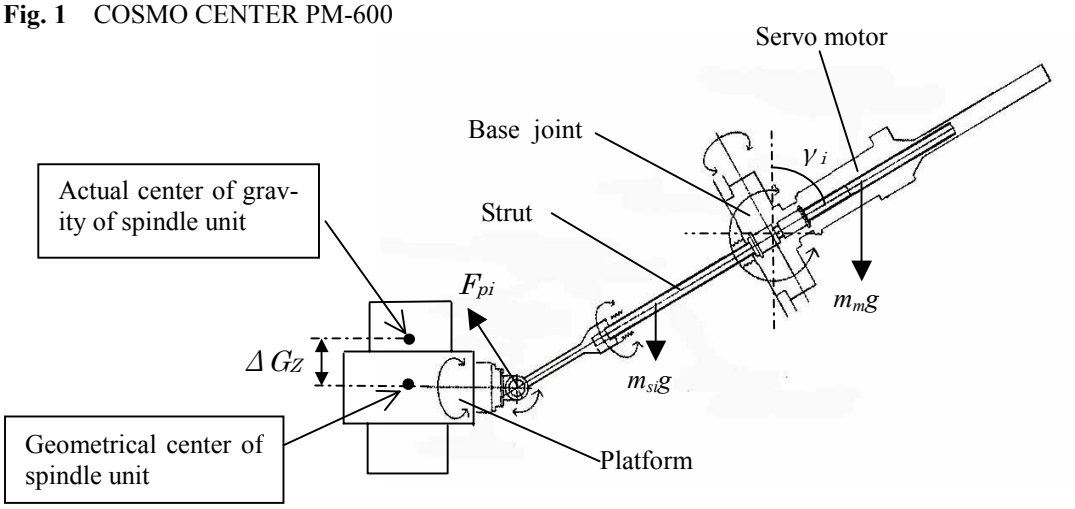

Fig. 2 Equilibrium of force and moment on a strut

3. Prediction of Gravity-induced Errors

3.1 Equilibrium of Force and Moment

This section presents a simulation model to predict the elastic deformation of mechanical parts due to the gravity. Since the effect of the bending of a strut on the machine's contouring error is much smaller than that of its axial deformation, the simulation model only considers the axial deformation of a strut. As illustrated in Figure 2, the model considers the gravity acting on a strut (of the mass m_{si}) and a servo motor (of the mass m_m). For the given position and orientation of the spindle, the objective is to estimate the force acting on each strut in the axial direction. Then, the positioning error at the tool tip is estimated as the superposition of the elastic axial deformation of each strut, which is proportional to the axial force imposed on it.

The axial force acting on the i-th strut, denoted by $\vec{F}_i$ (i = 1~6), is computed based on the equilibrium of force and moment. Since the only external force acting on this mechanism is the gravity, the equilibrium of force simply gives:

$$\sum_{i=1}^{6} \vec{F}_i = m_{mech} \cdot [0,\ 0,\ g]^T \tag{1}$$

where m_{mech} is the equivalent weight of the entire system (including the platform, spindle unit, 6 struts, and so on), and g denotes the gravity acceleration. The direction of $\vec{F}_i$ is the same as the direction of the i-th strut, and thus is a function of the position and orientation of the spindle.

On each strut, the gravity forces, $m_{si}g$ and m_mg, make the moment around the center of base joint (see Figure 2). This moment can be represented by the force, $\vec{F}_{pi}$, acting on the center of platform joint in the direction perpendicular to the i-th strut. It is given as follows:

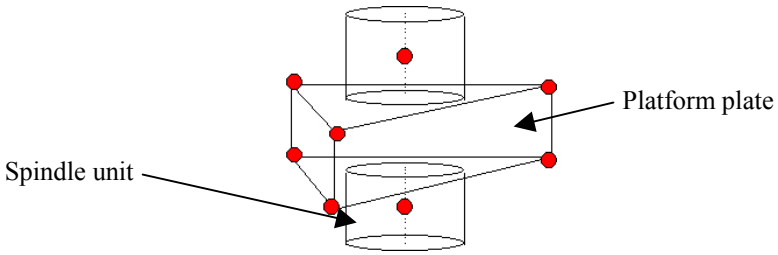

Fig. 3 Simplified model of platform and spindle unit

$$\left|\vec{F}_{pi}\right| = m_m g \cdot \sin\gamma_i \cdot \frac{L_m/2}{L_{si}} - m_{si} g \cdot \sin\gamma_i \cdot \frac{1}{2} \tag{2}$$

where γ_i is the angle between the i-th strut and the Z axis, L_m is the length of the servo motor, L_{si} is the length of the i-th strut (between the platform joint and the base joint). This equivalent force makes the torque around the center of gravity of the spindle unit as follows:

$$\vec{M}_s = \sum_{i=1}^{6} \left(\vec{F}_{pi} \times \vec{D}_{pi}\right) \tag{3}$$

where $\vec{D}_{pi}$ is the position vector of the i-th platform joint with respect to the center of gravity of the platform (including the platform plate and the spindle unit), and "×" denotes the outer product of two vectors. In addition to the weight of struts and servo motors, the weight of spindle unit itself also introduces the moment. For the simplification, the platform plate and the spindle unit are modeled as eight particles of the mass m_j (j = 1~8), as shown in Figure 3. When the platform plate is tilted, these weights give the following moment:

$$\vec{M}_p = \sum_{j=1}^{8} \left([0, 0, m_j]^T \times \vec{G}_j\right) \tag{4}$$

where $\vec{G}_j$ (j = 1~8) is the position vector of the j-th particle with respect to the center of gravity of the spindle unit. $\vec{G}_j$ is also a function of the tilting angle of the spindle. Note that the center of gravity is shifted by ΔG_z to the Z-direction from the geometrical center of the spindle unit, as shown in Figure 2. ΔG_z can be identified based on actual measurement of servo motor load. The details will be given in Section 3.2. The total moment given by the weight of the spindle unit, struts, and servo motors is:

$$\vec{M} = \vec{M}_s + \vec{M}_p \tag{5}$$

From the equilibrium of moment, each axial force on the i-th strut, $\vec{F}_i$ (i = 1~6), must satisfy the following equation:

$$\sum_{i=1}^{6} (\vec{F}_i \times \vec{D}_{pi}) = \vec{M} \tag{6}$$

By solving Eqs. (1) and (6), the axial force imposed on each strut, $\left|\vec{F}_i\right|$ (i = 1~6), can be computed for the given position and orientation of spindle.

The elastic deformation of the i-th strut in the axial direction is assumed to be proportional to $\left|\vec{F}_i\right|$. It can be written as follows:

$$\Delta L_i = K_{stiff}\left(\alpha L_i + C_B\right) \cdot \left|\vec{F}_i\right| \tag{7}$$

where C_B is the compliance of the ball screw in the axial direction, L_i is the length of the i-th strut (a function of the position and orientation of the spindle), and $\alpha = S \cdot E$ with the cross sectional area of the strut, S, and the Young's modulus, E. K_{Stiff} is a constant to compensate the stiffness of the strut, and is identified based on actual measurement of the machine's contouring error. Its identification will be also discussed in Section 3.2.

The positioning error at the tool tip is given as the superposition of the deformation of each strut. That is,

$$\vec{p} + \Delta\vec{p} = f(L_1 + \Delta L_1, \cdots, L_6 + \Delta L_6) \tag{8}$$

where $\vec{p}$ represents the commanded position and orientation of the tool, and $\Delta\vec{p}$ is the positioning and orientation error vector. f denotes the forward kinematic function of the Stewart platform parallel mechanism.

Table 2 Circular test conditions for the identification of simulation parameters

Condition	Center location of circle, mm			Radius, mm	Tilting angles of spindle, deg		
	X	Y	Z		a	b	c
A	0	100	-1008	144	-23	0	0
B	100	0	-1008	144	0	23	0

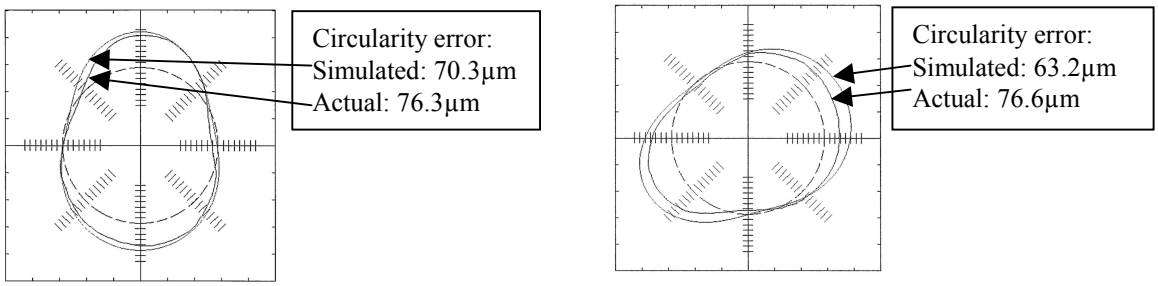

Center of circle: (0,100,-1008) mm,
Radius: 144mm,
Tilting angle: (-23°, 0°, 0°)

(a) A circular test on which the identification is based.

Center of circle: (-70,-70,-1008) mm,
Radius: 144 mm
Tilting angle: (17°, -17°, 0°)

(b) A circular test on which the identification is not based.

Fig. 4 Simulated and measured contouring error profiles

Table 3 Comparison of circularity error in measured and simulated circular test profiles

Condition	Center of circle, mm X, Y, Z	Radius, mm	Tilt angles, deg a,b,c	Circularity error, μm		Error, %
				Measured	Simulated	
A	0,100,-1008	144	-23,0,0	76.4	70.3	-8
B	100,0,-1008	144	0,23,0	35.6	27.1	-24
C	-70,-70,-1008	144	17,-17,0	63.2	76.6	21
D	0,100,-1008	144	-25,0,0	141.4	124.9	-12

3.2 Identification of Simulation Parameters

The model presented in the previous subsection includes the parameters that must be experimentally identified. When such parameters are properly identified, the model can predict gravity-induced motion errors in a sufficient accuracy despite of its simplicity. In particular, we identified two parameters, namely ΔG_z and K_{stiff}, based on actual measurement of servo motor currents and contouring error profiles in circular tests.

By monitoring the amateur current of six servo motors in a circular test, the load imposed on each strut can be estimated along the circular path. An equivalent total torque, $\vec{M}$ (see Eq. (6)), can be computed based on the measured load profiles. ΔG_z can be identified such that the error between simulated and measured load profiles is minimized.

The parameter K_{stiff} is identified based on contouring error profiles in a circular test. Throughout this paper, the circularity error is used as an index to evaluate the machine's motion accuracy. Based on multiple circular tests with a different center location and spindle orientation, K_{stiff} is identified such that the error between measured and simulated contouring error profiles is minimized. In our test, we performed two circular tests in the conditions shown in Table 2 for the identification of ΔG_z and K_{stiff}.

3.3 Simulation of Gravity-induced Errors

Based on the prediction of axial deformation of each strut, the positioning error at the tool tip can be simulated by using the forward kinematic function. Figure 4 (a) compares simulated and measured contouring error profiles in the condition A in Table 2. Note that for the identification of the two parameters was based on this profile. Figure 4 (b) compares simulated and measured contouring error profiles in the condition that is not used in the identification. The figures show a good agreement between simulated and measured profiles even in the latter case. As summarized in Table 3, the error between simulated and measured circularity errors is approximately 20% at maximum.

Table 4 Circularity errors with and without the gravity compensation

Condition	Center of circle, mm X, Y, Z	Radius, mm	Tilt angles, deg a, b, c	Circularity error, μm		Improvement, %
				Without compensation	With compensation	
A	0,100,-1008	144	-23,0,0	76.3	28.4	63
B	100,0,-1008	144	0,23,0	35.6	22.7	36
C	-70,-70,-1008	144	17,-17,0	63.2	15.9	75
D	0,100,-1008	144	-25,0,0	141.4	56.6	60
E	0,100,-1008	144	-20,0,0	37.9	10.7	72
F	0,100,-1008	144	-10,0,0	8.7	4.1	53
G	0,100,-1008	144	0,0,0	6.5	4.4	32
H	0,100,-1008	144	10,0,0	4.2	5.2	-24
I	0,100,-1008	144	23,0,0	6.8	6.5	4

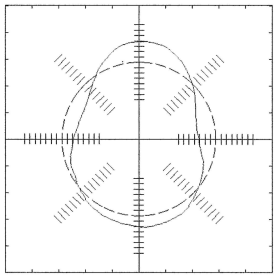

Circularity error: 76.3 μm

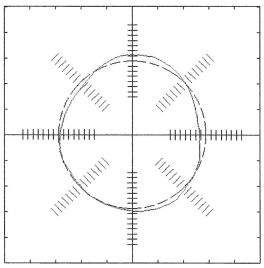

Circularity error: 28.4 μm

(a) Without compensation (b) With compensation

Center of circle: (0,100,-1008) mm,
Radius: 144 mm,
Tilting angles: (-23°,0°,0°)

Fig. 5 Compensation of gravity-induced contouring error

4. Compensation of Gravity-induced Errors

4.1 Compensation Scheme

The error induced by the gravity can be compensated by using the simulator presented above. At every 0.1° from the starting point on a circular path, the positioning error (ΔX_i, ΔY_i, ΔZ_i) (i = 1~3600) is simulated. Then, the reference circular trajectory is shifted by ($-\Delta X_i$, $-\Delta Y_i$, $-\Delta Z_i$) at every point.

4.2 Compensation Results

Table 4 compares circularity errors with and without the compensation in total eight conditions. "Improvement" in the table shows the percentage of the reduction in the circularity error by applying the compensation.

In all conditions shown in Table 4, the circularity error was significantly reduced. Recall that the simulation parameters ΔG_z and K_{Stiff} were identified based on the contouring error profiles measured in the conditions A and B, and thus it is reasonable to expect better compensation in these conditions. In other conditions where the gravity significantly deteriorates the circularity error (e.g. C, D, and E), however, a significant improvement in the circularity error by the compensation was also observed. Figure 5 shows contouring error profiles in the condition A with and without the compensation.

4.3 Discussion

Figure 6 summarizes circularity errors in the conditions A, D~I, where the tiling angle of the spindle varies from –25° to +23° with the same center location, (0,100,-1008) mm. "(expected)" shows the circularity error computed simply by taking the difference between simulated and measured contouring error profiles.

At this stage, it is not clear why the actual circularity error with the compensation is not as small as the expected value. It may be attributable to the calibration error of kinematic parameters. In order to simulate the contouring error due to the gravity in a sufficient accuracy, the calibration error of kinematic parameters must be minimized. Although the set of kinematic parameters that showed the best contouring performance so far was used in the tests above, it may still contain calibration errors to some extent. If the calibration error is further reduced, then further improvement by the gravity compensation is expected.

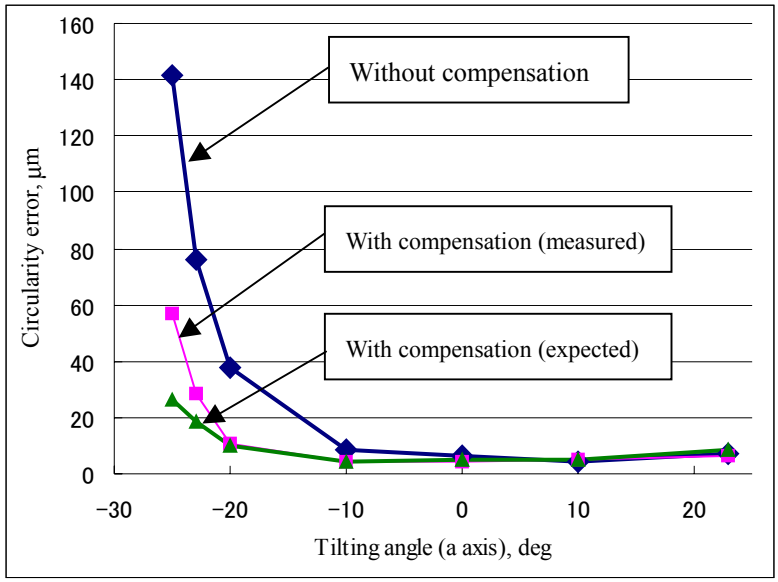

Fig. 6 Circularity error versus tilting angle

5. Conclusion

This paper presented a compensation scheme for gravity-induced contouring errors based on a motion simulator of a Hexapod-type parallel mechanism machine tool. The following conclusions are drawn:

(1) A simulator to predict gravity-induced errors is proposed based on the axial elastic deformation of struts. The simulation parameters are identified based on measured contouring error profiles and servo motor current profiles in circular tests. Simulated contouring error profiles showed a good agreement with measured ones. The error between simulated and measured circularity errors was approximately 20% at maximum.

(2) By compensating a reference trajectory based on the proposed simulator, the circularity error was reduced by about 70% at maximum when the tilting angle of the spindle around the X-axis is more than 20 degrees, where the gravity imposes a significant effect on the machine's contouring performance.

(3) In many cases, the reduction of circularity error by applying the gravity compensation was not as much as its expected value, i.e. the error between measured and simulated contouring error profiles. It may be attributable to the calibration error of kinematic parameters. For further effective compensation of gravity-induced contouring errors, the calibration error of kinematic parameters must be further reduced.

Acknowledgement

This research is partially supported by the Grant-in-Aid for Scientific Research of JSPS (#15560094).

References

(1) Nakagawa, M., Matsushita, T., Nashiki, M., Kakino, Y., Ihara, Y., A Study on the Improvement of Motion Accuracy of Hexapod type Parallel Mechanism Machine Tool (1st Report), *Journal of the Japan Society for Precision Engineering*, Vol.67, No.8(2001), pp.1333-1337.

(2) Kakino, Y., Ihara, Y., Shinohara, A., *Accuracy Inspection of NC Machine Tools by Double Ball Bar Method*, Carl Hanser Verlag(1993).

(3) M.Weck, D. Staimer, Accurcy Issues of Parallel Kinematic Machine Tools, Compensation and Calibration, *Proc. of 2000 Parallel Kinematic Machines Int. Conf.*,(2000) pp.35-41.

(4) Soons, J. A., Measuring the Geometric Errors of a Hexapod Machine Tool, *Proceedings of the Lamdamap Conference*, Newcastle, United Kingdom (1999), pp. 169-182.

(5) Stewart, D., A Platform with six degree of freedom, *Proceedings of the Institution of Mechanical Engineering*, Vol. 180, Part 1, No. 15(1965), pp. 371-386.

(6) M. Nakagawa, T. Matsushita, S. Watanabe, Y. Kakino, Y. Ihara：The Improvement of Motion Accuracy of Hexapod Type Machine Tools and Its Machining Performance, *Proc. of 2002 Japan-USA Symposium on Flexible Automation* (2002), pp. 979-982.